Science Advances
AAAS

Supplementary Materials for

Robust dynamic brain coactivation states estimated in individuals

Xiaolong Peng *et al.*

Corresponding author: Email: Hesheng Liu, hesheng@biopic.pku.edu.cn

Sci. Adv. **9**, eabq8566 (2023)
DOI: 10.1126/sciadv.abq8566

This PDF file includes:

Supplemental Experimental Procedures

Data preprocessing

For *Dataset VII*, the "minimally processed" fMRI data were employed. The "minimal" preprocessing steps included: 1) gradient distortion correction; 2) motion correction; 3) readout distortion correction; 4) registration to the T1 scan; 5) spline resampling to FSL MNI152 2mm space using FSL FNIRT; and 6) intensity normalization to a mean of 10,000 and bias field correction. The conventional resting state fMRI processing procedure was then applied to the "minimally preprocessed" data, which included: 1) projecting the data from the FSL MNI152 space onto the FreeSurfer fsaverage6 surface space (2 mm mesh, 40962 vertices in each hemisphere); 2) linear detrending and band-pass filtering (0.01-0.08Hz); 3) regressing nuisance variables including the global signal, the six parameters obtained by rigid body head motion correction, and their first temporal derivatives; 4) spatial smoothing with a 6 mm FWHM Gaussian curve; 5) down-sampling the BOLD fMRI data to the FreeSurfer fsaverage4 surface space (2562 vertices in each hemisphere) using the mri_surf2surf function provided by FreeSurfer; 6) temporal normalization was then applied to the signal extracted from each vertex.

Group-level coactivation pattern (Group CAP) analysis

For the Group CAP analysis, we followed the same procedure as described in our previous work (*1*), which was revised slightly from the original Group CAP method (*2*). Briefly, preprocessed fMRI data from the same dataset was concatenated to form a large data matrix. Principal component analysis (PCA) was then performed to reduce the dimension of the combined data to improve the computational efficiency. The criterion for PCA was that the down-sampled features can still explain 90% of the total variance of the original data. Note that, this PCA procedure was not included in the original Group CAP analysis in Liu's study (*2*). However, it is a necessary pre-step for clustering on large fMRI datasets, which takes up huge computing resources. A k-means clustering algorithm was then applied to classify the fMRI time frames into different clusters based on spatial similarity, resulting in multiple spontaneous coactivation patterns, or brain states. In the present study, cluster number was also set to 16 for ease of comparison among different methods.

Hidden Markov Model – Multivariate Autoregressive (HMM-MAR) analysis

For the HMM-MAR analysis, the HMM-MAR toolbox (https://ohba-analysis.github.io/osl-docs/pages/overview/overview_hmm.html) was applied, which has been previously employed to temporally decompose the brain states from the HCP dataset (*3*). In the present study, we used the same parameter settings as those used in Vidaurre's study (i.e., PCA component number = 50, repetitions = 3). Number of brain states was also set to 16 for ease of comparison among different methods.

Comparison of reliability at the individual level

We compared the test-retest reliability in occurrence rate of brain states derived from three methods, our INSCAPE approach, Group CAP and HMM-MAR. The comparisons were carried out in two independent datasets – HCP unrelated 100-subject dataset (*Dataset VII*) and CoRR-HNU 30-subject dataset (*Dataset II*). While the Group CAP method yielded low test-retest reliability (Mean ± SEM, 0.5593 ± 0.0303 and 0.6825 ± 0.0439 in HCP and CoRR-HNU, respectively), the test-retest reliability was much higher for the INSCAPE approach (Mean ± SEM, 0.7222 ± 0.0173 and 0.8956 ± 0.0131). The improvement in reliability was statistically significant (see *Fig. S9*; Paired t-test, HCP: ***$p < 0.0001$, t = 5.9726; CoRR-HNU: ***$p < 0.0001$, t = 4.6049). The HMM-MAR approach showed comparable test-retest reliability as the INSCAPE approach in both HCP dataset (Mean ± SEM, HMM-MAR: 0.6931 ± 0.0289; Paired t-test, $p = 0.3882$, t = 0.8648) and CoRR-HNU dataset (Mean ± SEM, HMM-MAR: 0.8976 ± 0.0187; Paired t-test, $p = 0.3882$, t = 0.0780). However, HMM-MAR suffers from poor generalizability across different datasets, as will be described below.

Comparison of generalizability across datasets

Since both the INSCAPE approach and HMM-MAR approach showed promising test-retest reliability in occurrence rate, we further compared these two methods in terms of spatial characteristics. We derived group-level brain states from the HCP and CoRR-HNU datasets, respectively. Group-level brain states derived from these two datasets using our INSCAPE approach showed consistent spatial patterns (*Fig. S10*; mean spatial similarity: r = 0.7753, all $p < 0.0001$). However, group-level brain states derived from these two datasets using the HMM-MAR approach barely correspond to each other (*Fig. S11*). When brain states were sorted according to spatial similarity, only four state pairs showed a spatial similarity greater than 0.5 and the mean spatial similarity was relatively low (r = 0.3499). These results indicated that the HMM-MAR approach does not capture stable group-level brain states across different datasets thus the findings from one dataset can hardly be generalized to a different dataset.

Comparison of computational efficiency

We compared the computational cost of all three dynamic methods (i.e., Group Cap, HMM-MAR, and INSCAPE) in the HCP dataset (n = 100) and CoRR-HNU dataset (n = 30). All analyses were carried out on the same DELL workstation (Inter Xeon Silver 4112 CPU, 32 GB RAM), under the same OS environment (Linux Centos 7) and using the same MATLAB (R2022a). Compared to our INSCAPE method, the processing times of Group CAP and HMM-MAR were respectively 56 times and 5 times longer for HCP dataset, and 36 times and 10 times longer for CoRR-HNU dataset (see *Fig. S12*). Note that for Group CAP and HMM-MAR approaches, we only calculated the time needed for clustering analysis, without counting the time for the PCA procedure prior to clustering. Both Group CAP and HMM-MAR methods require combining the whole dataset first and down-sample with PCA before the clustering analysis. This procedure

is computationally expensive, e.g., PCA procedure for HCP unrelated 100 subjects took about 27.7 min. The time needed for PCA could grow exponentially as the sample size increases. In contrast, our INSCAPE approach directly applies the precalculated group template to decode the brain state of any new subject and does not require analyzing the new dataset as a group, thus it is computationally efficient and not limited by sample size.

Quantification of the head motion effect on INSCAPE

We performed additional analyses to explore how head motion affects the occurrence rate of brain states. We applied our INSCAPE approach to 154 GSP subjects who were previously excluded due to high level of head motion. We ran a parallel analysis on these subjects after scrubbing the frames with a head motion greater than 0.5 mm. The mean motion (FD) was significantly lower after scrubbing (see *Fig. S13a*, paired t-test, $p < 0.0001$). Interestingly, we found no significant difference in occurrence rate of brain states after scrubbing (see *Fig. S13b*). We also quantified the similarity of occurrence rate in each individual pre- and post-motion scrubbing. We found that all subjects showed a similarity over 98% (see *Fig. S13c*). One possible explanation is that head motion did not occur during any specific brain state but occurred with equal chance in all states. Finally, the spatial similarity of each brain state across 154 subjects was over 99.93% (see *Fig. S13d*), indicating that when head motion is not excessive (as in this example), we could still decode the brain states relatively reliably.

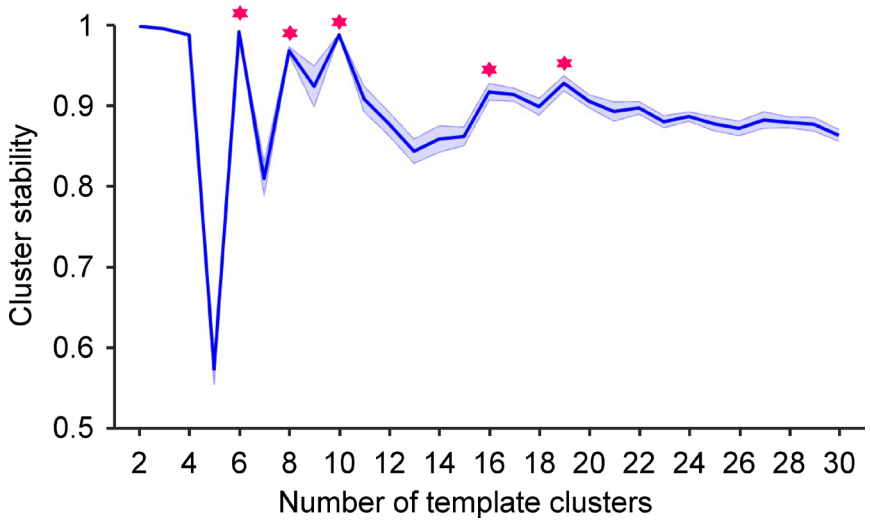

Fig. S1.

Determination of the optimal cluster number based on test-retest stability of brain states. Within-subject test-retest stability of the clustering algorithm was used to optimize the number of brain states. Half of the resting-state runs were randomly selected from each of the 846 subjects from *Dataset I* and assigned to the test group, with the other half assigned to the retest group. The stability of the clustering analysis was estimated as the mean spatial similarity of brain states derived from the test and retest groups. This test-retest procedure was repeated 100 times. Mean stability (dark blue curve) and ±SEM (blue shadowed areas) across the 100 repetitions are plotted. Several local maxima on the curve were identified (marked with red stars), suggesting that solutions of 6, 8, 10, 16, and 19 clusters were relatively stable. In this study, we selected 16 clusters for further analyses since it balanced the test-retest reliability with the diversity of the brain states.

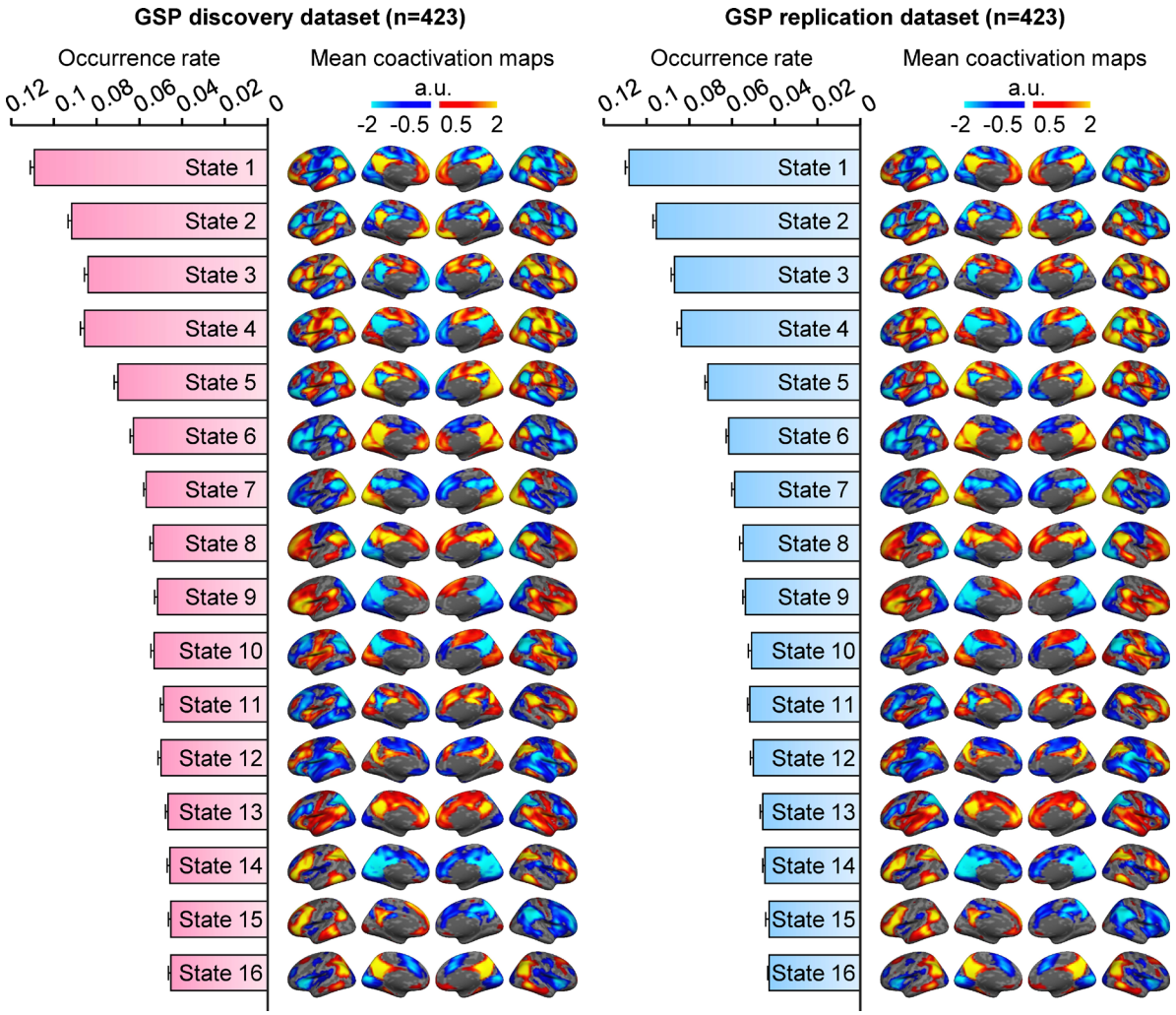

Fig. S2.

The occurrence rate and mean coactivation maps of dynamic brain states are highly consistent between the discovery and replication samples. To test the reliability of our INSCAPE approach, the occurrence rate and mean coactivation maps of the 16 brain states were estimated independently in half of the GSP dataset (*Dataset I*), which was designated as the discovery sample (n = 423) and replicated in the other half of the dataset that was designated as the replication sample (n = 423). The discovery and replication occurrence rates of the 16 brain states were highly consistent (Pearson correlation, $r = 0.995$, $p < 0.001$). Moreover, the discovery and replication mean coactivation maps of the 16 brain states also showed highly significant spatial similarity (mean spatial similarity, $r = 0.992$, $p < 0.001$).

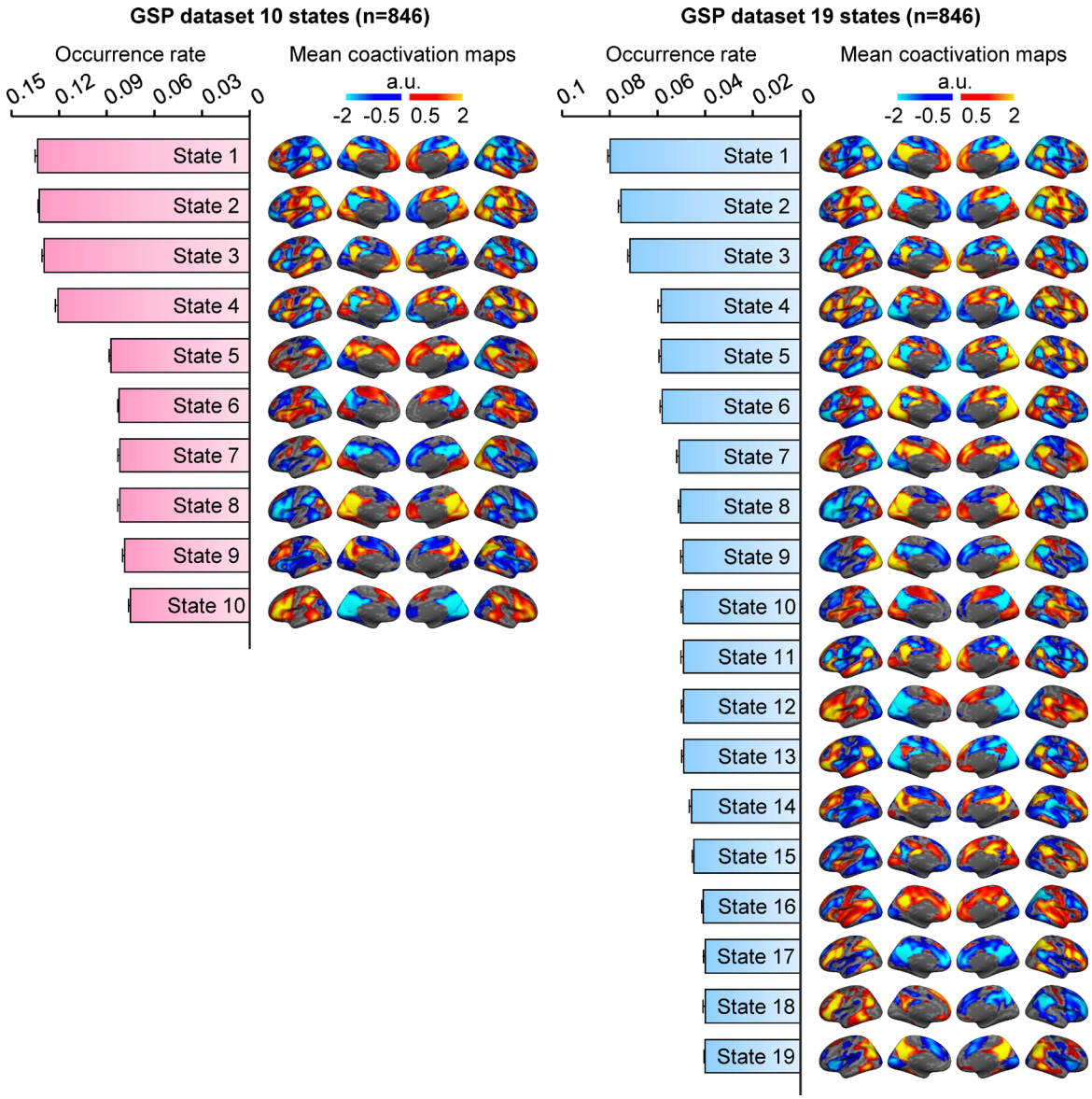

Fig. S3.

Characterization of the occurrence rates and mean coactivation maps of brain states derived from the 10- and 19-cluster solutions. The occurrence rate and mean coactivation maps derived from the 10- and 19-cluster solutions were estimated in the GSP dataset (*Dataset I*; n = 846). Although the 19-cluster solution has more clusters than the 10-cluster solution, both shared similar mean coactivation maps and distributions of occurrence rates. For example, the mean coactivation maps of the first four brain states with the highest occurrence rate were observed in both the 10- and 19-cluster solutions. Additional brain states in the 19-cluster solution appeared to be further subdivisions of brain states identified in the 10-cluster solution.

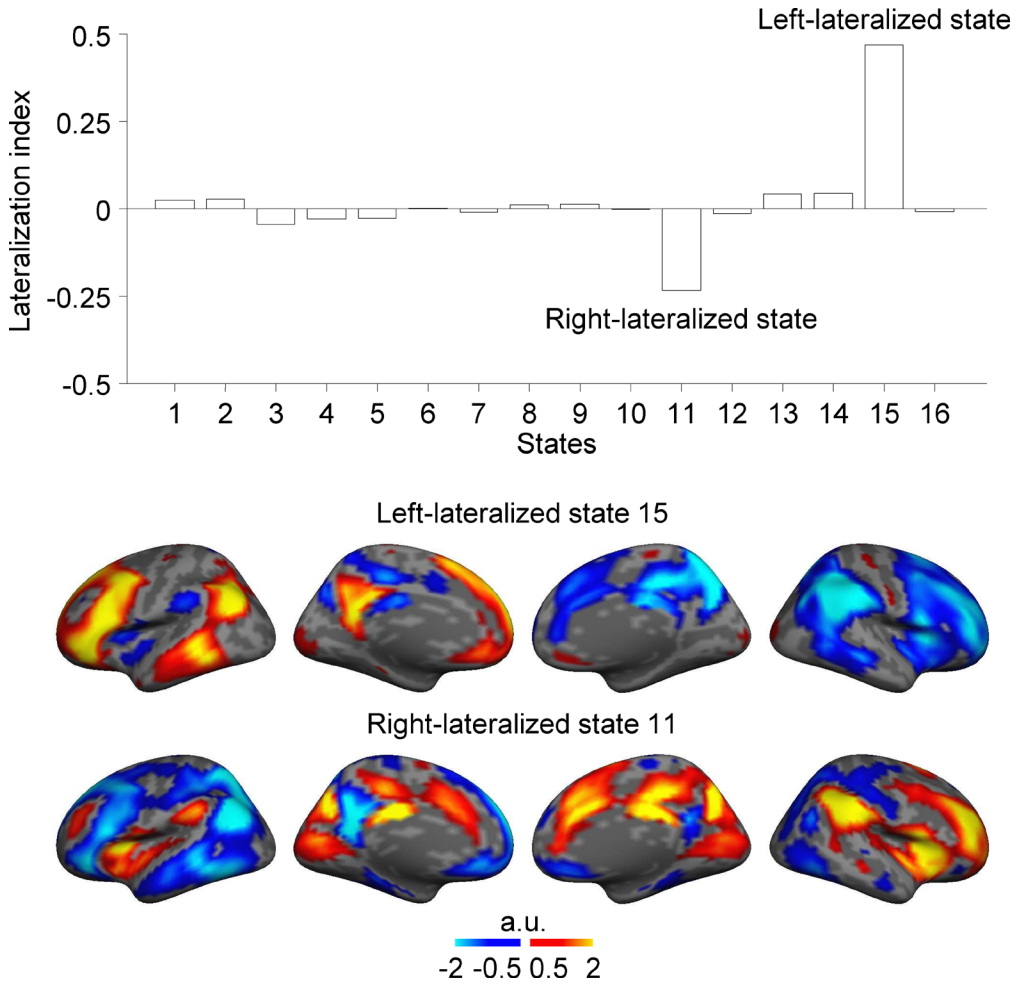

Fig. S4.

Lateralized brain states were selected according to the lateralization index between the left and right hemispheres. The mean coactivation maps of 16 brain states were projected to a FreeSurfer symmetric cortical inflated surface template, consisting of 2,562 vertices per hemisphere. The lateralization index was defined as the difference in the number of activated vertices between the left and right hemispheres divided by the total number of vertices in a given hemisphere. The lateralization indices of the 16 brain states were plotted with positive values indicating left-lateralization and negative values indicating right-lateralization. State 15 showed the highest lateralization index and therefore was selected as the left-lateralized brain state, while state 11 showed the lowest lateralization index and was chosen as the right-lateralized brain state. The mean coactivation maps of the left- and right-lateralized brain states 15 and 11, respectively, are shown in the bottom panel.

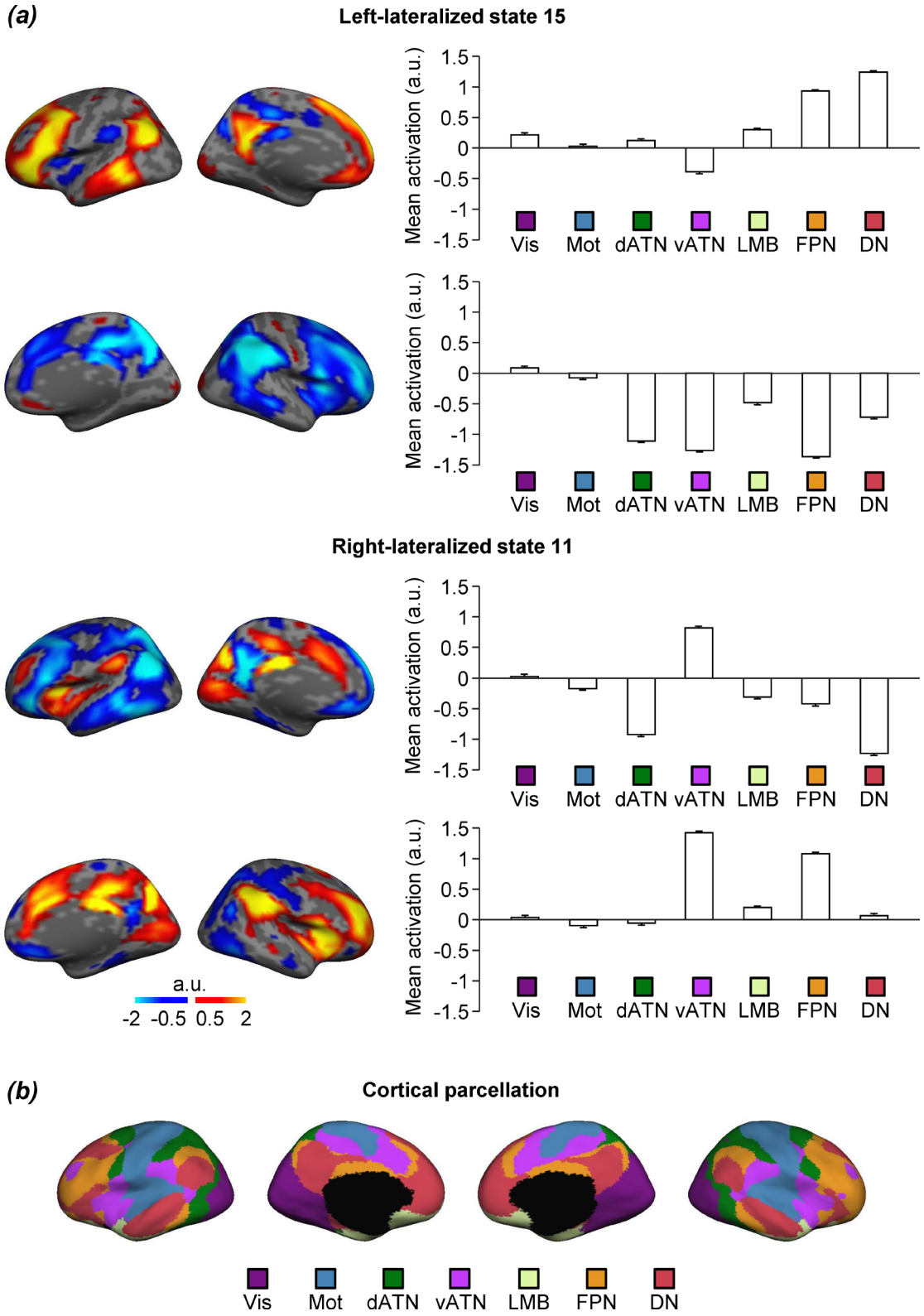

Fig. S5.

Lateralization of brain states was quantified across seven canonical cerebral networks in each hemisphere. The mean coactivation maps of left-lateralized state 15 and right-lateralized state 11 were compared with the 7-network cortical parcellation previously employed by Yeo et al (*4*). (a) The mean

coactivation maps for left-lateralized brain state 15 (top panel) and right-lateralized brain state 11 (bottom panel) are shown along side bar graphs displaying the mean coactivations (±SEM) averaged within each of the 7 networks for the left and right hemisphere. (b) The 7-network cortical parcellations projected onto the medial and lateral cortical surface of the left and right hemispheres, which are color-coded to denote network classification. The 7 networks included the visual network (Vis; purple), somatomotor network (Mot; blue), the dorsal (dATN; green) and ventral (vATN; violet) attention networks, limbic network (LMB; cream), frontoparietal control network (FPN; orange) and default mode network (DN; red). Note that left-lateralized state 15 showed the strongest activation in DN and FPN in the left hemisphere and deactivation in FPN, vATN, and dATN in the right hemisphere. Right-lateralized state 11 demonstrated the greatest activation in the vATN bilaterally and in the right FPN, whereas deactivation in DN and dATN in the left hemisphere was observed.

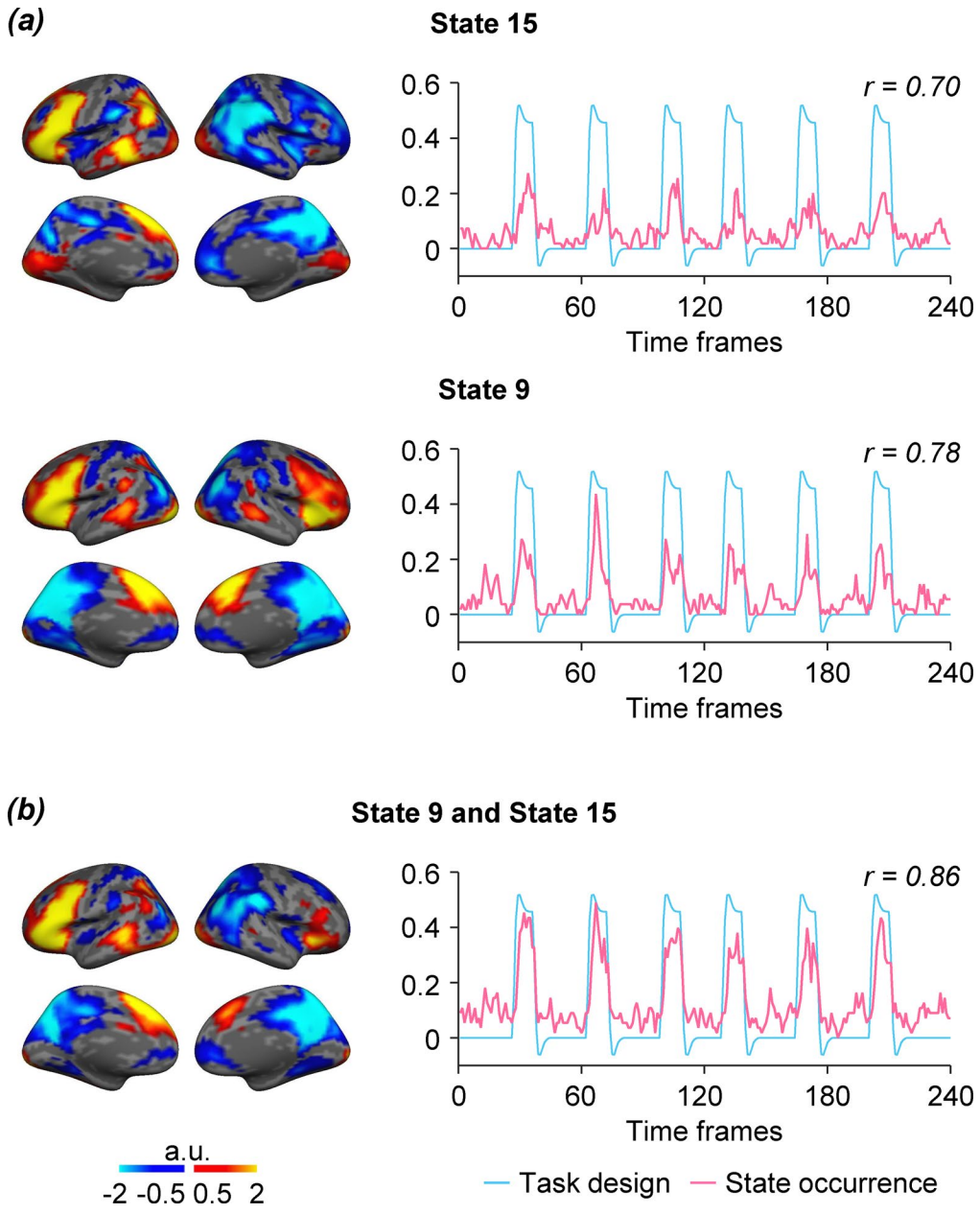

Fig. S6.

The occurrence of task-related brain states was frequently coincident with task onset. (a) The occurrence rate of the 16 brain states was quantified in the language task dataset (*Dataset III*), which contained 55 healthy, adult subjects. The occurrence of each brain state was calculated across subjects at each time point during the language task to generate an occurrence curve of each brain state. Then the state occurrence curve was compared with the hemodynamic response curves of task onsets. The brain state 15 and state 9 showed significant correlation with the task onsets indicating these two states might be involved in the language task processing (Pearson correlation, state 15: $r = 0.70$, $p < 0.001$, state 9: $r = 0.78$, $p < 0.001$). (b) The brain state 9 and state 15 were then combined as a language-related brain state to calculate its mean coactivation maps and state occurrence curve. The combined brain state has activations in the traditional language areas. The occurrence curve of this combined state is significantly correlated with the hemodynamic response curves of language task onsets (Pearson correlation, $r = 0.86$, $p < 0.001$).

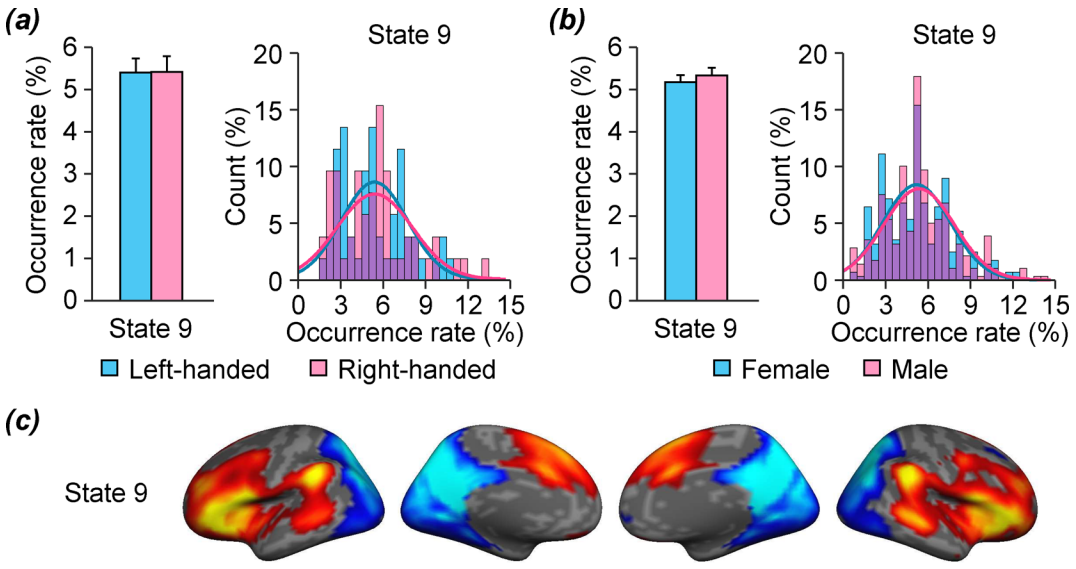

Fig. S7.

Language-related brain state 9 is not affected by handedness and gender. In addition to left-lateralized brain state 15, our findings also indicated that brain state 9 was involved in language-related processing. We therefore examined the influence of handedness and gender on the occurrence of brain state 9. (a) The mean occurrence rate (±SEM) of brain state 9 was estimated in 52 left-handed (blue bars) and 52 demographically matched right-handed (pink bars) subjects taken from *Dataset IV*. No difference was found between left- and right-handed subjects (paired t-test, $p = 0.965$). The occurrence rate distributions for state 9 are depicted in a histogram denoting left-handed by blue bars and right-handed subjects by pink bars, with the overlap shown in purple. Gaussian curves fit the distributions, demonstrating no difference between left- and right-handed subjects (Kolmogorov-Smirnov test, $p = 0.858$). (b) The mean occurrence rates of brain state 9 (±SEM) in 279 males (pink bars) and 279 demographically matched females (blue bars). No difference was found between males and females (paired t-test, $p = 0.420$). The occurrence rate distributions of state 9 are displayed in female (blue bars) and male (pink bars) subjects demonstrates no difference in occurrence rate distributions (Kolmogorov-Smirnov test, $p = 0.523$). (c) Mean coactivation map for state 9 from the group template projected onto the medial and lateral inflated cortical surface of the left and right hemisphere.

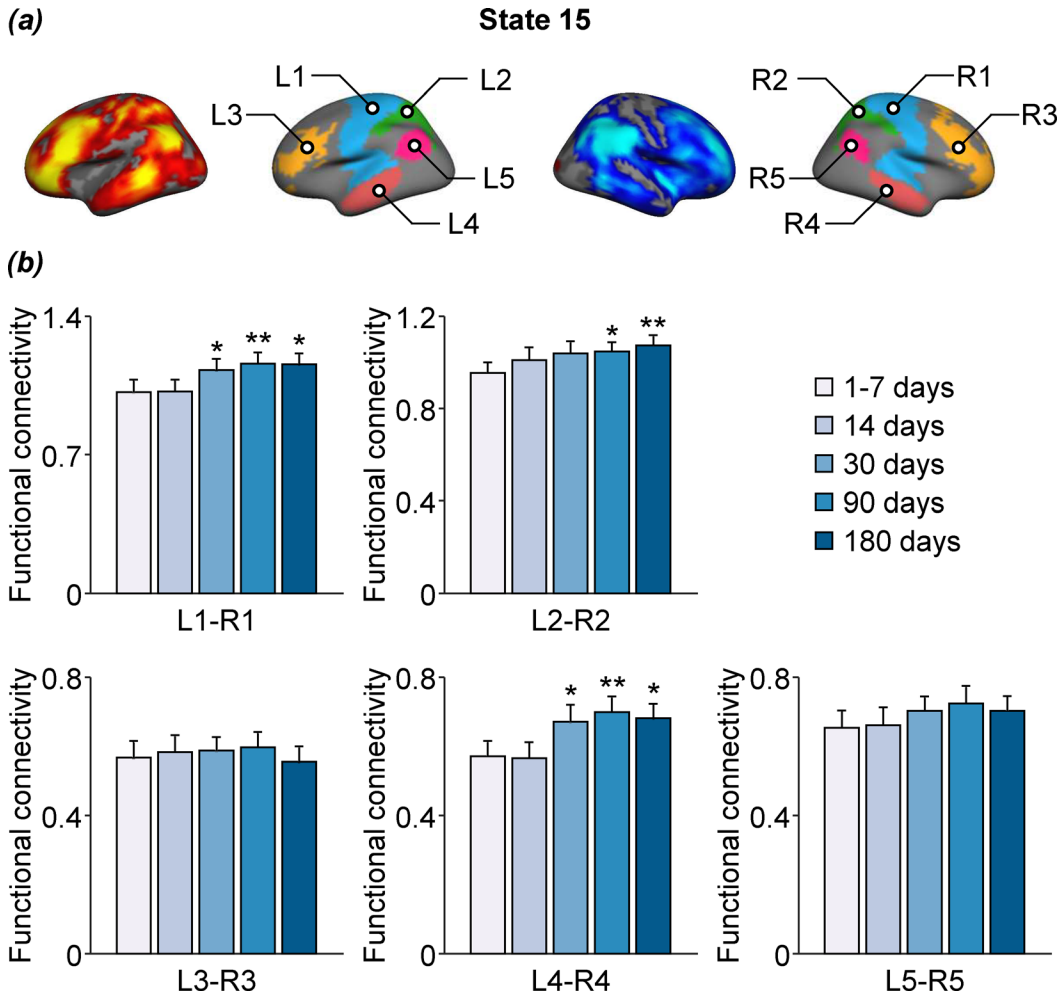

Fig. S8.

Between-hemisphere functional connectivity changes in patients with subcortical stroke during the first six months of recovery. (a) The five left-hemispheric patches (L1, L2, L3, L4, and L5) with the highest activations in brain state 15 at the 1-7 day post-stroke time point and the five symmetric patches (R1, R2, R3, R4, and R5) from the right hemisphere were selected as ROIs to evaluate changes in the inter-hemispheric connectivity at 14, 30, 90 and 180 days post-stroke relative to the baseline time point (1-7 days post-stroke). (b) Static functional connectivity of patch-pairs L1-R1 and L4-R4 showed significant increases over time (repeated-measures ANOVA, $p < 0.05$) at 30, 90, and 180 days post-stroke compared with baseline (paired t-test, $^{*}p < 0.05$, $^{**}p < 0.01$). In addition, static functional connectivity showed a significant increase for the L2-R2 patch pair at 90 and 180 days post-stroke. No significant differences in static functional inter-hemispheric connectivity for the L3-R3 and L5-R5 patch-pairs across the 5 post-stroke time points were found.

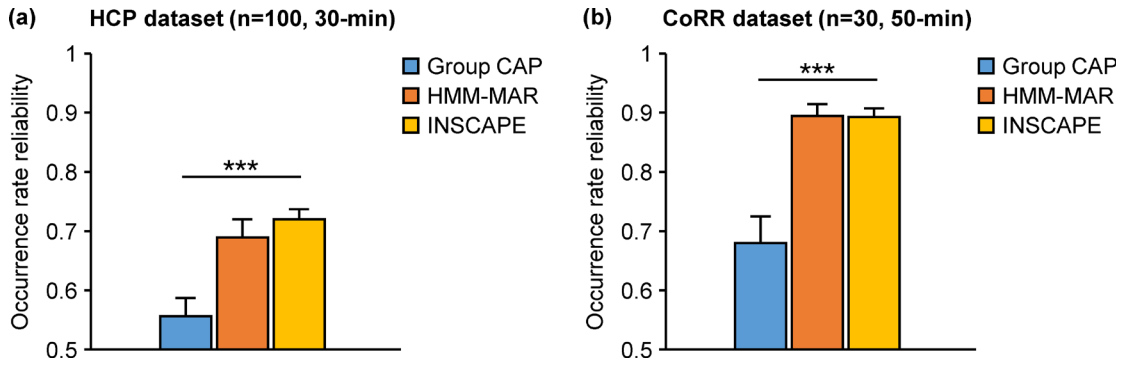

Fig. S9.

Comparison of reliability among three different methods for brain dynamics analysis. The test-retest reliability in occurrence rate of brain states derived from out INSCAPE approach was compared with two previous reported dynamic analysis methods – Group CAP and HMM-MAR. The comparisons were carried out in two independent datasets – (a) HCP unrelated 100-subject dataset (supplemental *Dataset VII*) and (b) CoRR-HNU 30-subject dataset (*Dataset II*). Our INSCAPE approach showed much higher test-retest reliability than the Group CAP method (Paired t-test, HCP: ***$p < 0.0001$, t = 5.9726; CoRR-HNU: ***$p < 0.0001$, t = 4.6049). The HMM-MAR approach showed comparable test-retest reliability as the INSCAPE approach in both HCP dataset (Paired t-test, $p = 0.3882$, t = 0.8648) and CoRR-HNU dataset (Paired t-test, $p = 0.3882$, t = 0.0780).

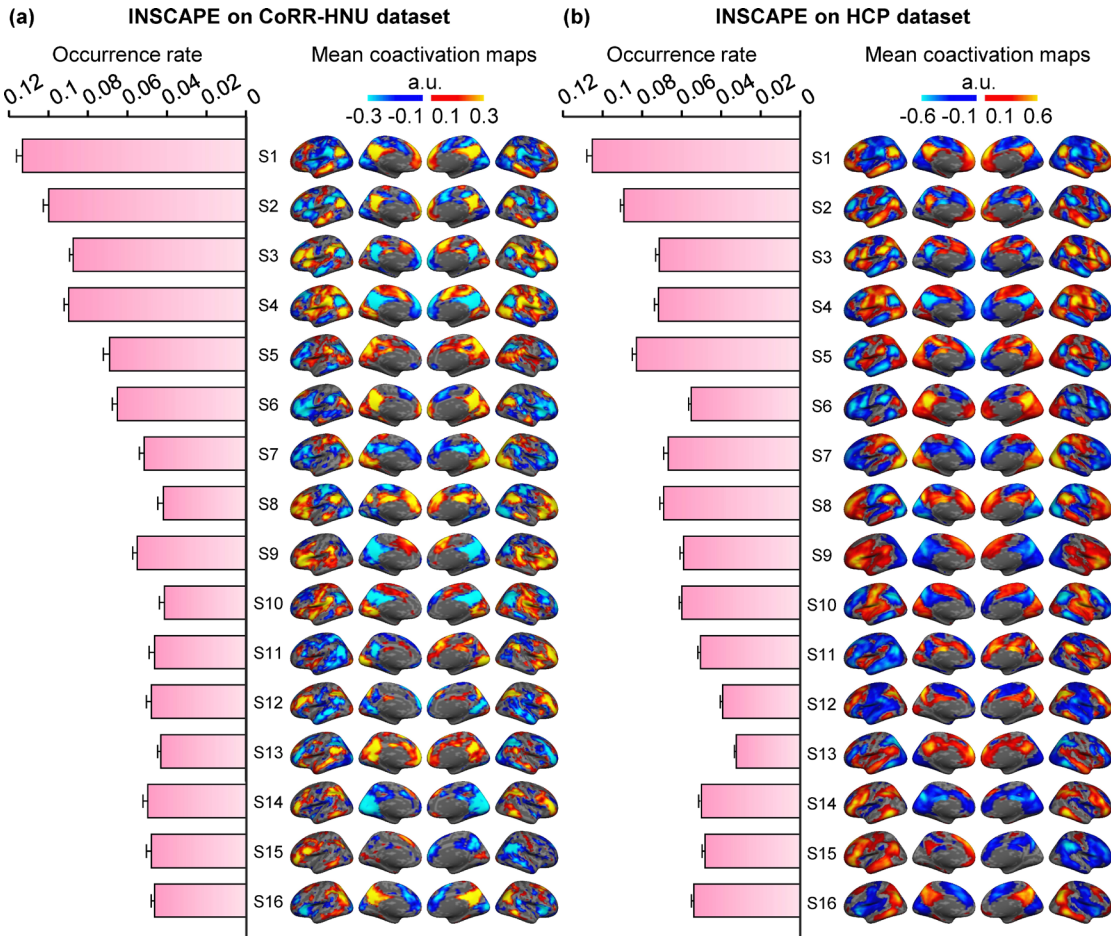

Fig. S10.

INSCAPE identifies consistent group-level brain states across different datasets. Group-level brain states were estimated using the INSCAPE approach from the (a) CoRR-HNU dataset and (b) HCP dataset. Brain states derived from these two datasets showed consistent spatial patterns in all 16 brain states (mean spatial similarity: $r = 0.7753$, all $p < 0.0001$).

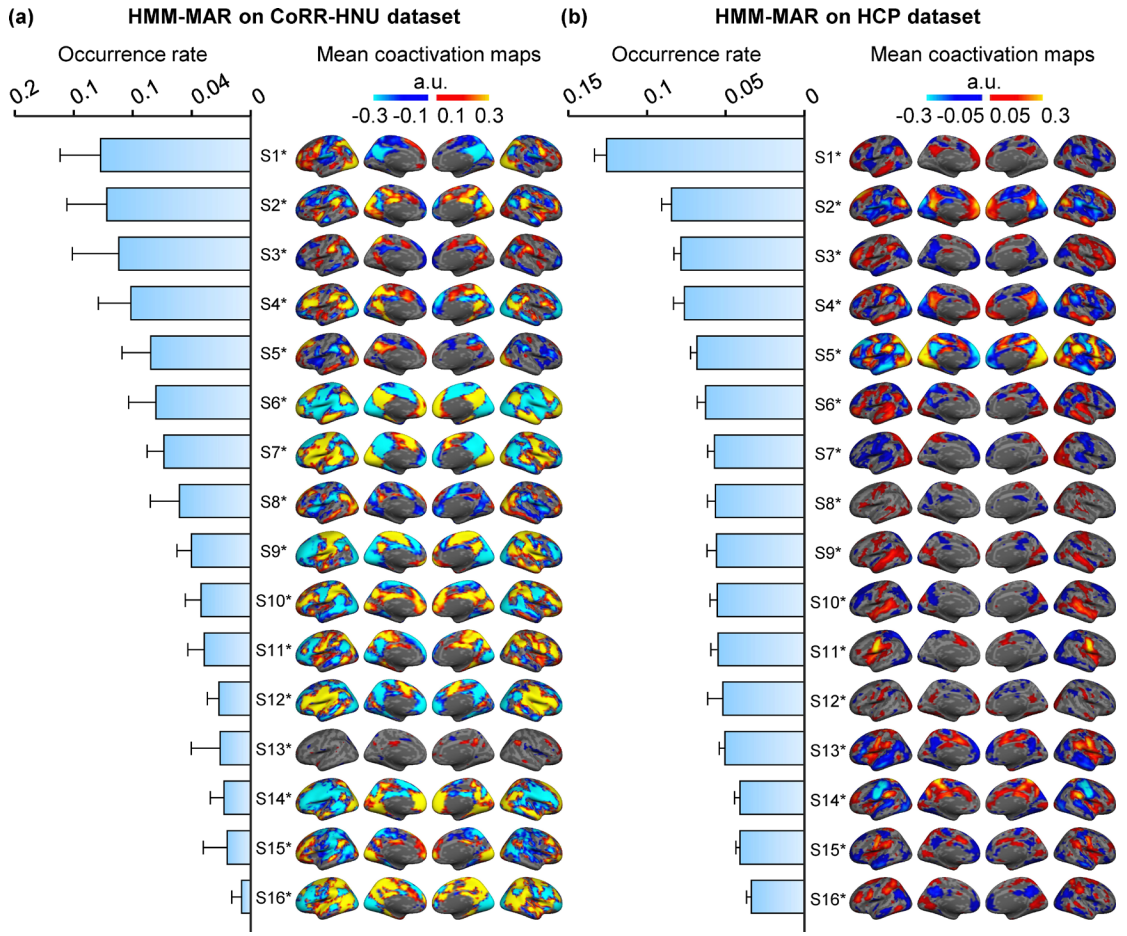

Fig. S11.

HMM-MAR approach identifies inconsistent group-level brain states across datasets. Brain states were estimated using the HMM-MAR approach in the (a) CoRR-HNU dataset and (b) HCP dataset, respectively. Group-level brain states derived from these two datasets were inconsistent. (Mean spatial similarity across state pairs with highest spatial similarity: 0.3499).

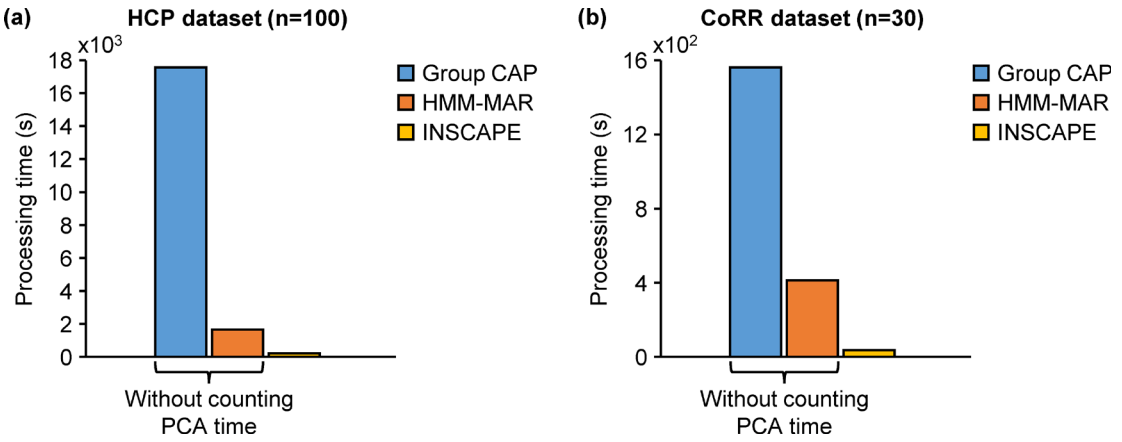

Fig. S12.

Comparison of computational efficiency. We compared the computational cost of three dynamic methods (i.e., Group Cap, HMM-MAR, and INSCAPE) in the (a) HCP dataset (n = 100) and (b) CoRR-HNU dataset (n = 30). All analyses were carried out on the same computational environment. For Group CAP and HMM-MAR approaches, we only calculated the time needed for clustering analysis, without counting the time for the PCA procedure prior to clustering (e.g., PCA procedure for HCP unrelated 100 subjects took about 27.7 min). Compared to our INSCAPE method, the processing times of Group CAP and HMM-MAR were respectively 56 times and 5 times longer for HCP dataset, and 36 times and 10 times longer for CoRR-HNU dataset.

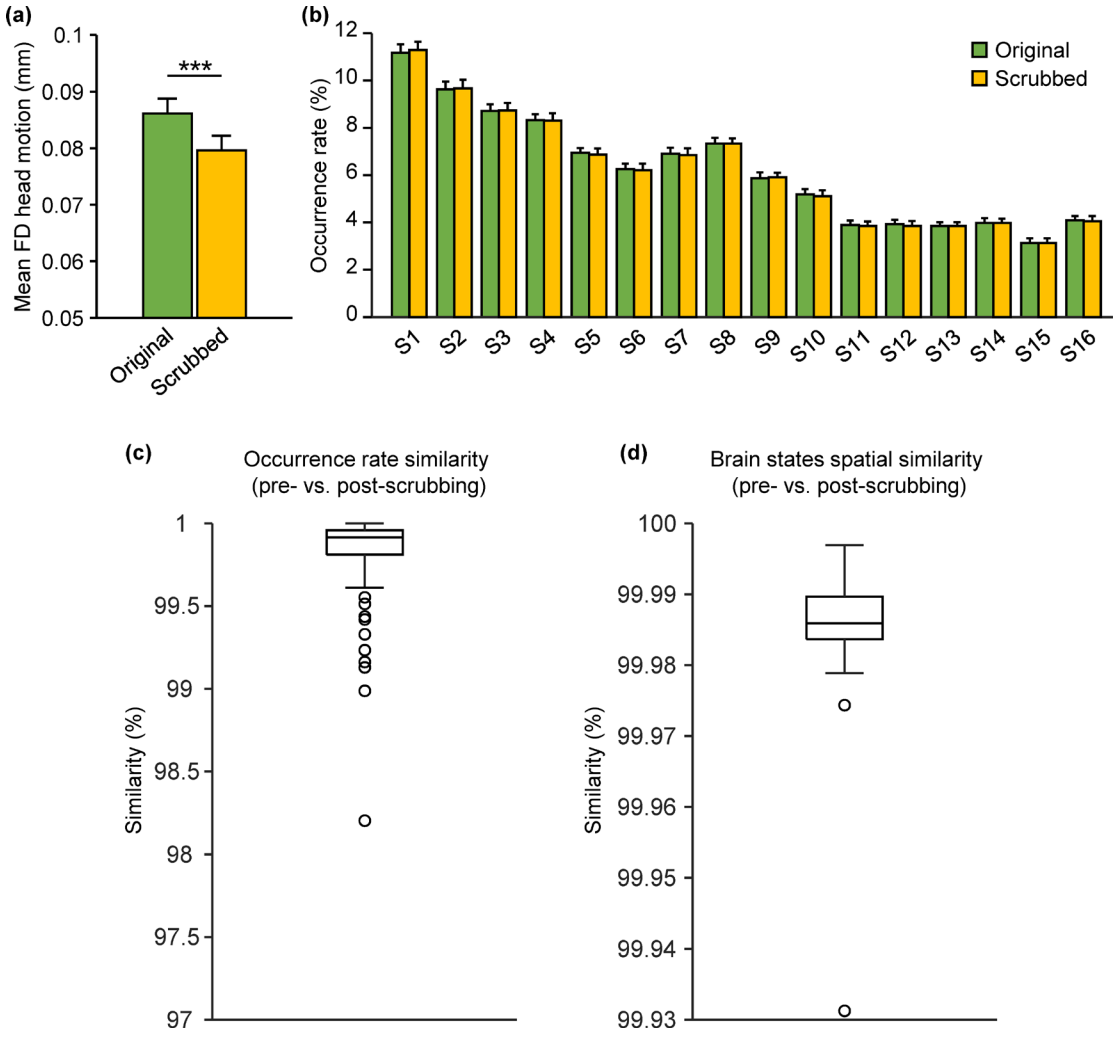

Fig. S13.

INSCAPE approach is robust to the effect of head motion. The INSCAPE approach was applied to 154 GSP subjects who were previously excluded from the template generation due to high level of head motion. A parallel analysis was performed on these subjects after scrubbing the frames with a head motion greater than 0.5 mm. (a) The mean head motion (FD) was significantly lower after scrubbing (Paired t-test, $p < 0.0001$). (b) No significant difference in occurrence rate of brain states was found after scrubbing. (c) For all subjects, the similarity of occurrence rate in each individual pre- and post-motion scrubbing was over 98%. (d) The spatial similarity of each brain states across 154 subjects was over 99.93%.